
Inductive Graph Neural Networks for Spatiotemporal Kriging

Yuankai Wu
McGill University
yuankai.wu@mail.mcgill.ca

Dingyi Zhuang
McGill University
dingyi.zhuang@mail.mcgill.ca

Aurelie Labbe
HEC Montreal
aurelie.labbe@hec.ca

Lijun Sun
McGill University
lijun.sun@mcgill.ca

Abstract

Time series forecasting and spatiotemporal kriging are the two most important tasks in spatiotemporal data analysis. Recent research on graph neural networks has made substantial progress in time series forecasting, while little attention is paid to the kriging problem—recovering signals for unsampled locations/sensors. Most existing scalable kriging methods (e.g., matrix/tensor completion) are transductive, and thus full retraining is required when we have a new sensor to interpolate. In this paper, we develop an Inductive Graph Neural Network Kriging (IGNNK) model to recover data for unsampled sensors on a network/graph structure. To generalize the effect of distance and reachability, we generate random subgraphs as samples and reconstruct the corresponding adjacency matrix for each sample. By reconstructing all signals on each sample subgraph, IGNNK can effectively learn the spatial message passing mechanism. Empirical results on several real-world spatiotemporal datasets demonstrate the effectiveness of our model. In addition, we also find that the learned model can be successfully transferred to the same type of kriging tasks on an unseen dataset. Our results show that: 1) GNN is an efficient and effective tool for spatial kriging; 2) inductive GNNs can be trained using dynamic adjacency matrices; and 3) a trained model can be transferred to new graph structures.

1 Introduction

With recent advances in information and communications technologies (ICT), large-scale spatiotemporal datasets are collected from various applications, such as traffic sensing and climate monitoring. Analyzing these spatiotemporal datasets has attracted considerable attention. Time series forecasting and spatiotemporal kriging are two essential tasks in spatiotemporal analysis [1, 2]. While recent research advances in deep learning have made substantial progress in time series forecasting (e.g., [3, 4, 5]), little attention is paid to the spatiotemporal kriging application. The goal of spatiotemporal kriging is to perform signal interpolation for unsampled locations given the observed signals from sampled locations during the same period. The interpolation results can produce a fine-grained and high-resolution realization of spatiotemporal data, which can be used to enhance real-world applications such as travel time estimation and disaster evaluation. In addition, a better kriging model can achieve higher estimation accuracy/reliability with less number of sensors, thus reducing the operation and maintenance cost of a sensor network.

For general spatiotemporal kriging problems (e.g., in Euclidean domains), a well-developed approach is Gaussian process (GP) regression [1, 6], which uses flexible kernel structure to characterize

spatiotemporal correlations. However, GP has two limitations: (1) the model is computationally expensive and thus it cannot deal with large-scale dataset, and (2) it is difficult to model networked systems using existing graph kernel structures. To solve large-scale kriging problems in a networked system, graph regularized matrix/tensor completion has emerged as an effective solution (e.g., [2, 7, 8, 9]). Combining low-rank structure and spatiotemporal regularizers, these models can simultaneously characterize both global consistency and local consistency in the data. However, matrix/tensor completion is essentially transductive: for new sensors/nodes introduced to the network, we cannot directly apply a previously trained model; instead, we have to retrain the full model for the new graph structure even with only minor changes (i.e., after introducing a new sensor). In addition, the low-rank scheme is ineffective to accommodate time-varying/dynamic graph structures. For example, some sensors may retire over time without being replaced, and some sensors may be introduced at new locations. In such cases, the network structure itself is not consistent over time, making it challenging to utilize the full information.

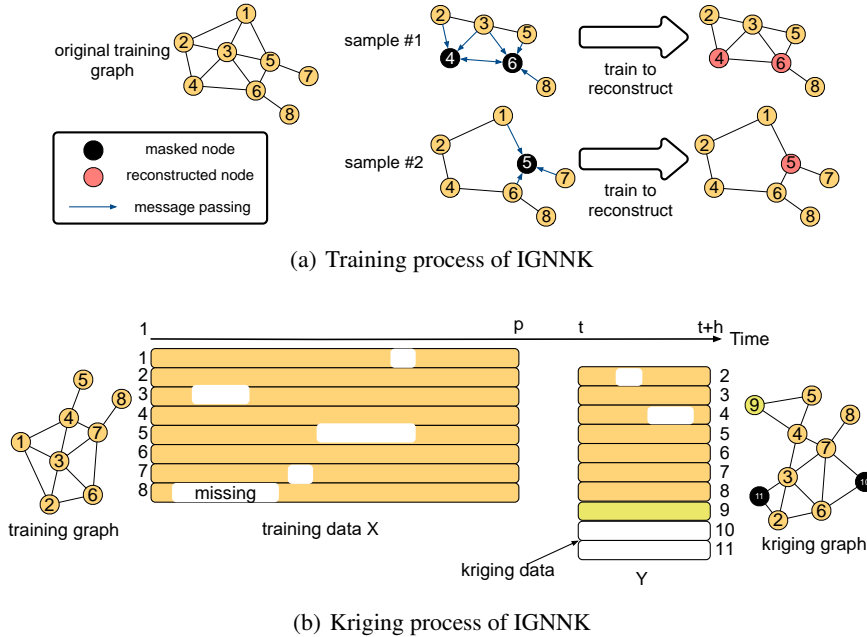


Figure 1: Framework of IGNNK. (a) In sample #1, nodes $\{1, 7\}$ are unsampled and nodes $\{4, 6\}$ are masked and used for reconstruction. In sample #2, The unsampled set and masked set are $\{3\}$ and $\{5\}$, respectively. (b) Illustration of real-time kriging, where the goal is to perform interpolation for virtual sensors $\{10, 11\}$. Note that the set of observed sensor during $[t, t + h]$ is not necessary the same as the set during training $[1, p]$. For example, during $[t, t + h]$, the sensor $\{1\}$ in X is removed and a new sensor $\{9\}$ (in green) is added to the network.

Recent research has explored the potential of modeling spatiotemporal data using Graph Neural Network (GNN). GNNs are powerful in characterizing complex spatial dependencies by its message passing mechanism [10]. They also demonstrate the ability and inductive power to generalize the message passing mechanism to unseen nodes or even entirely new (sub)graphs [11, 12, 13]. Inspired by these works, here we develop an Inductive Graph Neural Network Kriging (IGNNK) model to solve real-time spatiotemporal kriging problems on dynamic network structures. Different from graphs in recommender systems governed by certain typology, our spatial graph actually contains valuable location information which allows us to quantify the exact pairwise “distance” beyond “hops”. In particular, for directed networks such as highway network, the distance matrix will be asymmetric and it actually captures the degree of “reachability” from one sensor to another [14, 15]. To better leverage the distance information, IGNNK trains a GNN with the goal of reconstructing information on random subgraph structures (see Figure 1). We first randomly select a subset of nodes from all available sensors and create a corresponding subgraph. We mask some of them as missing and train the GNN to reconstruct the full signals of all nodes (including both the observed and the masked nodes) on the subgraph (Figure 1(a)). This training scheme allows GNN to effectively learn

the message passing mechanism, which can be further generalized to unseen nodes/graphs. Next, given observed signals from the same or even an entirely new network structure, the trained model can perform kriging through reconstruction (Figure 1(b)).

We compare IGNNK with other state-of-the-art kriging methods on five real-world spatiotemporal datasets. IGNNK achieves the best performance on all datasets, suggesting that the model can effectively generalize spatiotemporal dynamics on a sensor network. To demonstrate the transferability of IGNNK, we apply the trained models from two traffic speed datasets (METR-LA and SeData) to a new one (PeMS-Bay), and we find that the two models offer very competitive performance even when the new dataset is never seen.

2 Related work

The network spatiotemporal kriging problem can be considered a special matrix completion problem in which several rows are completely missing. A common solution is to leverage the network structure as side information [7, 16]. In a spatiotemporal setting, network kriging is similar to the problems presented in [2, 8, 9, 17]. Low-rank tensor models are developed by capturing dependencies among variables [2] or incorporating spatial autoregressive dynamics [9]. Different from previous approaches, we try to gain inductive ability using GNN. Our method is closely related the following research directions.

GNNs for spatiotemporal datasets Graph Convolutional Networks (GCNs) are the most commonly used GNN. The generalized convolution operation on graph is first introduced in [18]. Deferrard et al. [19] proposes to use Chebyshev polynomial filters on the eigenvalues to approximate the convolutional filters. Kipf et al. [20] further simplifies the graph convolution operation using the first-order approximation of Chebyshev polynomial. To model temporal dynamics on graphs, GCNs are combined with recurrent neural networks (RNNs) and temporal convolutional networks (TCNs). One of the early methods using GCNs to filter inputs and hidden states in RNNs is [21]. Later studies have integrated different convolution strategies, such as diffusion convolution [14], gated convolution [22], attention mechanism [23], and graph WaveNet [24]. As these models are essentially designed for temporal forecasting problems, they are not suitable for the spatiotemporal kriging task.

Inductive GNNs Hamilton et al. [11] is the first to show that GNNs are capable of learning both *transductive* and *inductive* node representations. Some recent studies have developed inductive GNNs for recommender systems by extracting user/item embeddings on the user-item bipartite graphs. For example, Zhang et al. [25] masks a part of the observed user and item embeddings and trains a GCN to reconstruct these masked embedding. Zhang and Chen [26] uses local graph patterns around a rating (i.e., an observed entry in the matrix) and builds one-hop subgraph to train a GCN, providing inductive power to generalize to unseen users/items and transferability. Zeng et al. [13] proposes a graph sampling approach to construct subgraphs to train GNN for large graphs. The full GNN trained using sampled subgraphs shows superior performance. More recently, Appleby et al. [17] develops a kriging convolutional networks (KCN), which construct a local subgraph by nearest neighbor algorithm, and train a GNN to reconstruct each individual node’s static label. However, the nearest neighbor approach (i.e., local structure) in these studies might be insufficient and ineffective in generalizing the global patterns and the effect of distance in spatial networks and spatiotemporal data [2, 14]. In addition, KCN ignores the fact that the labels of the node is temporally evolving in spatiotemporal datasets.

3 Methodology

3.1 Problem description

Spatiotemporal kriging refers to the task of interpolating/recovering time series/signals at unsampled locations/sensors given signals from sampled locations/sensors. We use the terms “node”, “sensor”, and “location” interchangeably throughout the paper. This study focuses on spatiotemporal kriging on networks: the spatial domain becomes an irregular network structure instead of a 2D surface. Consider a set of traffic sensors on a highway network as an example: we can model the sensors as nodes in a network, and the edges can be defined based on the typology of the highway network [14].

In this case, the objective of spatiotemporal kriging is to recover traffic state time series at locations with no sensors. Thus, kriging can be considered the process of setting up virtual sensors. We illustrate the real-time network kriging problem in Figure 1(b). Let $[t_1, t_2] = \{t_1, t_1 + 1, \dots, t_2 - 1, t_2\}$ denote a set of time points. Suppose we have data from n sensors during a historical period $[1, p]$ ($n = 8$ in Figure 1(b), corresponding to sensors $\{1, \dots, 8\}$). We denote by a multivariate time series matrix $X \in \mathbb{R}^{n \times p}$ the available data, with each row being the signal collected from a sensor. We use X as training data. Let $[t, t + h) = \{t, t + 1, \dots, t + h - 1\}$ be the period that we will perform kriging. During this period, assume we have data $Y_t^s \in \mathbb{R}^{n_t^s \times h}$ available from n_t^s sensors ($n_t^s = 8$ in Figure 1(b), corresponding to sensors $\{2, \dots, 9\}$), and we are interested in interpolating the signals $Y_t^u \in \mathbb{R}^{n_t^u \times h}$ on n_t^u virtual sensors (i.e., new/unsampled nodes, corresponding to sensors $\{10, 11\}$ in Figure 1(b)). Note that both X and Y_t^s might be corrupted with missing values. Moreover, it is possible that $n \neq n_t^s$ as some sensors may retire and new sensors may be introduced. Our goal is to estimate Y_t^u given Y_t^s . To achieve this, we design IGNNK to learn and generalize the message passing mechanism in training data X .

3.2 Subgraph signals and random masks

As a first step of IGNNK, we develop a sampling procedure—Algorithm 1—to generate a set of subgraphs for training. The key idea is to randomly sample a subset of nodes to get X_{sample} and build the corresponding adjacency matrix W_{sample} . The kriging problem is very different from applications in recommender systems, where the graph encodes only topological information (i.e., social network or co-purchasing network). In the spatial setting, our graph is essentially fully connected, in which we expect edge weight diminishes with Euclidean/travel distance between a pair of nodes. To better characterize the effect of “distance”, we simply choose a purely random sampling scheme to generate sample subgraphs, instead of creating a local subgraph for each node [11, 17]. We create a mask matrix M_{sample} to keep some nodes as observed and the rest as “unsampled”. We then use the generated masks M_{sample} , graph signals X_{sample} and adjacency matrix W_{sample} to train a GNN. The input data X_{sample} itself could contain missing values, which we will also mark as unknown. This will enable IGNNK to perform spatial interpolation under missing data scenarios.

Algorithm 1 Subgraph signal and random mask generation

Require: Historical data X from sampled locations over period $[1, p]$ (size $n \times p$).

Parameters: window length h , sample size each iteration S , and maximum iteration I_{max} .

for iteration = 1 : I_{max} **do**

for sample = 1 : S **do**

 Generate random integers n_o (number of nodes selected as observed) and n_m (number of nodes selected as missing) with $n_o + n_m \leq n$.

 Randomly sample $n_o + n_m$ indices without replacement from $[1, n]$ to obtain $I_{\text{sample}} = \{i^1, \dots, i^{n_o}, \dots, i^{n_o+n_m}\}$.

 Randomly choose a time point j within range $[1, p - h]$. Let $J_{\text{sample}} = [j, j + h]$.

 Obtain submatrix signal $X_{\text{sample}} = X[I_{\text{sample}}, J_{\text{sample}}]$ with size of $(n_o + n_m) \times h$.

 Construct adjacency matrix $W_{\text{sample}} \in \mathbb{R}^{(n_o+n_m) \times (n_o+n_m)}$ for nodes in I_{sample} .

 Generate a mask matrix M_{sample} of size $(n_o + n_m) \times h$, $M_{\text{sample}}[i, :] = \begin{cases} 1, & \text{if } i \in [1, n_o], \\ 0, & \text{otherwise.} \end{cases}$

end for

 Use sets $\{X_{1:S}\}, \{M_{1:S}\}, \{W_{1:S}\}$ to train GNNs.

end for

3.3 GNN architecture

The second step of IGNNK is to train a GNN model to reconstruct the full matrix X_{sample} on the subgraph given the incomplete signals $X_{\text{sample}}^M = X_{\text{sample}} \odot M_{\text{sample}}$, where \odot denotes Hadamard product. In order to achieve higher forecasting power, previous studies mainly combine GNNs with sequence-learning models—such as RNNs and TCNs—to jointly capture spatiotemporal correlations, in particular long-term temporal dependencies. However, for our real-time kriging task, the recovery windows h is relatively short. Therefore, we simply assume that all time points in the recovery window h are correlated with each other, and model a length- h signal as h features.

Real-world spatial networks are often directed with a asymmetric distance matrix (see e.g., [15]). To characterize the stochastic nature of spatial and directional dependencies, we adopt the Diffusion Graph Convolutional Networks (DGCNs) [14] as the basic building block of our architecture:

$$H_{l+1} = \sum_{k=1}^K T_k(\bar{W}_f) H_l \Theta_{b,l}^k + T_k(\bar{W}_b) H_l \Theta_{f,l}^k, \quad (1)$$

where $\bar{W}_f = W_{\text{sample}} / \text{rowsum}(W_{\text{sample}})$ and $\bar{W}_b = W_{\text{sample}}^T / \text{rowsum}(W_{\text{sample}}^T)$ are the forward transition matrix and the backward transition matrix, respectively; Here we use two transition matrices because the adjacency matrix can be asymmetrical in a directional graph. In an undirected graph, $\bar{W}_f = \bar{W}_b$. K is the order of diffusion convolution; the Chebyshev polynomial is used to approximate the convolution process in DGCN, and we have $T_k(X) = 2XT_{k-1}(X) - T_{k-2}(X)$ defined in a recursive manner with $T_0(X) = I$ and $T_1(X) = X$; $\Theta_{f,l}^k$ and $\Theta_{b,l}^k$ are learning parameters of the l th layer that control how each node transforms received information; H_{l+1} is the outputs of the l th layer. Unlike traditional GNNs using a fixed spatial structure, in IGNNK each sample has its own subgraph structure. Thus, the adjacency matrices W_{sample} capturing neighborhood information and message passing direction are also different in different samples.

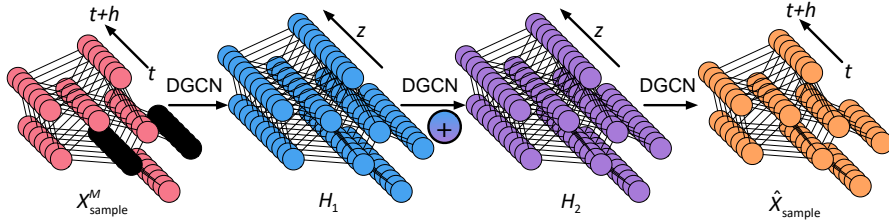


Figure 2: Graph neural network structure of IGNNK

Figure 2 illustrates the whole graph neural networks structure of IGNNK, which is a simple 3-layer DGCN. The input to the first layer is the masked signals $H_0 = X_{\text{sample}}^M$. Next, we set H_1 follow Eq. (1) with parameters $\Theta_{b,0}^k \in \mathbb{R}^{h \times z}$ and $\Theta_{f,0}^k \in \mathbb{R}^{h \times z}$. Since the masked nodes only pass 0 to its neighbors in the first layer, a one-layer GCN cannot produce desirable features. Therefore, we add another layer of DGCN (i.e., H_2) to produce more generalized representations:

$$H_2 = \sigma \left(\sum_{k=1}^K T_k(\bar{W}_f) H_1 \Theta_{b,1}^k + T_k(\bar{W}_b) H_1 \Theta_{f,1}^k \right) + H_1, \quad (2)$$

where $\Theta_{f,1}^k \in \mathbb{R}^{z \times z}$ and $\Theta_{b,1}^k \in \mathbb{R}^{z \times z}$ are parameters of the second layer DGCN, and $\sigma(\cdot)$ is a nonlinear activation function. The reason we add H_1 to H_2 is that H_1 contains the information about sensors with missing data.

After obtaining the final graph representation, we use another DGCN to output the reconstruction:

$$\hat{X} = \sum_{k=1}^K T_k(\bar{W}_f) H_2 \Theta_{b,2}^k + T_k(\bar{W}_b) H_2 \Theta_{f,2}^k, \quad (3)$$

where $\Theta_{f,2}^k \in \mathbb{R}^{z \times h}$ and $\Theta_{b,2}^k \in \mathbb{R}^{z \times h}$ are learning parameters of the last layer. Note that we keep the structure of IGNNK as parameter-economic as possible. One can always introduce more complex structures to further improve model capacity and performance.

3.4 Loss function and prediction

As stated in Section 3.1, the problem we addressed here is to recover the information of unsampled sensors. A straightforward approach is to define training loss functions only on the masked signals. However, from a methodological perspective, we prefer IGNNK to be generalized to both dynamic graph structures and the unseen nodes [11]. To make the learned message passing mechanism more

generalized for all nodes, we use the total reconstruction error on both observed and unseen nodes as our loss function:

$$J = \sum_{\text{sample}} \|\hat{X}_{\text{sample}} - X_{\text{sample}}\|_F^2. \quad (4)$$

We next illustrate how to perform kriging to get matrix Y_t^u for the virtual sensors in Figure 1(b). First, we can create the $(n_t^s + n_t^u) \times h$ binary mask matrix M_t and the $(n_t^s + n_t^u) \times (n_t^s + n_t^u)$ adjacency matrix W_t given the typology of the sensor network during $[t, t + h)$. Then, we can feed W_t and the “masked” signals $Y_t^M = [Y_t^s; Y_t^u]$ with $Y_t^u = \mathbf{0}$ to the trained IGNNK model to get $\hat{Y}_t^M = [\hat{Y}_t^s; \hat{Y}_t^u]$. The estimation $\hat{Y}_t^u \in \mathbb{R}^{n_t^u \times h}$ is the final kriging results for those virtual sensors.

4 Numerical experiments

In this section, we assess the performance of IGNNK using five real-world spatiotemporal datasets from diverse applications: (1) **METR-LA** is a traffic speed dataset from 207 sensors in Los Angeles over four months (Mar 1, 2012 to Jun 30, 2012); (2) **NREL** registers solar power output by 137 photovoltaic power plants in Alabama state in 2006; (3) **USHCN** contains monthly precipitation of 1218 locations from 1899 to 2019; (4) **SeData** is also a traffic speed dataset collected from 323 loop detectors in Seattle highway network; (5) **PeMS-Bay** is traffic speed dataset similar to METR-LA, which consists of traffic speed time series of 325 sensors in the Bay Area from Jan 1, 2017 to May 13, 2017. We use PeMS-Bay to demonstrate the transferability of IGNNK. The frequency for METR-LA, NREL, SeData and PeMS-Bay are all 5-min. In terms of adjacency structure, we compute the pairwise Euclidean distance matrices for NREL and USHCN; both METR-LA and PeMS-Bay have a travel distance-based adjacency matrix (i.e., “reachability”) which are asymmetric; SeData has a simple binary adjacency matrix (1 if two sensors are neighbors and 0 otherwise). We summarize the detailed information and the rules/methods to construct adjacency matrices for each dataset in Appendix A.

4.1 Experiment setup

Our implementation of IGNNK is available at <https://github.com/Kaimaoge/IGNNK>. We compare the performance of IGNNK with the following widely used kriging/interpolation and matrix/tensor factorization models. (1) **kNN**: K-nearest neighbors, which estimates the information of unknown nodes by averaging the values of the K spatially closest sensors on the network. (2) **OKriging**: ordinary kriging—a well-developed spatial interpolation model [1]. (3) **KPMF**: Kernelized Probabilistic Matrix Factorization, which incorporates graph kernel information [7] into matrix factorization using a regularized Laplacian kernel. (4) **GLTL**: Greedy Low-rank Tensor Learning, which is a transductive tensor factorization model for spatiotemporal cokriging [2]. GLTL deals with multiple variable using a $[location \times time \times variable]$ tensor structure. We implement a reduced matrix version of GLTL, as we only have one variable for all the datasets. (5) **sRMGCNN** [27], a transductive matrix completion framework uses GCNs to learn graph features. The model is designed for recommender systems, but it can be easily applied to kriging as a matrix completion problem.

To evaluate the performance of different models, we randomly select $\approx 25\%$ nodes as “unsampled” locations/virtual sensors (n_t^s) and keep the rest as observed for all the five datasets. For IGNNK, we take data from the first 70% time points as a training set X and test the kriging performance on the following 30% time points. For simplification, we keep the values of n_m and n_0 fixed in our implementation, instead of generating random numbers as in Algorithm 1. We choose $h = 24$ (i.e., 2 h) for the three traffic datasets, $h = 16$ (i.e., 80 min) for NREL, and $h = 6$ (i.e., 6 months) for USHCN. We perform kriging by a rolling-window approach on: $[t, t + h)$, $[t + h, t + 2h)$, $[t + 2h, t + 3h)$, etc. It should be noted that, since the training and test nodes are both given in the datasets, we can pre-compute the pairwise adjacency matrix for all nodes and obtain W_{sample} by directly selecting a submatrix from the full adjacency matrix. The detailed configuration of IGNNK is given in Appendix B. For matrix/tensor-based models (i.e., KPMF, GLTL and sRMGCNN), we use the entire dataset as input but mask the same 25% “unsampled” nodes as in IGNNK. We use the first 70% time points from unsampled nodes as a validation set to select the optimal hyperparameters, and evaluate recovery performance on the following 30% time points. For these models, the recovery for all the 30% test can be generated at once, and they use more information compared with IGNNK. The

full Gaussian process model for spatiotemporal kriging is computationally very expensive. Thus, we implement OKriging and kNN for each time step t separately (i.e., $h = 1$ without considering temporal dependencies). Again, we use the first 70% time points from the unsampled sensors for validation and the rest 30% for test. All the baseline models are tuned using validation (see Appendix C). Since OKriging uses the longitude/latitude as input, it is not appropriate for road-distance-based transportation networks. Therefore, OKriging is only applied to NERL and USHCN datasets. As the adjacency matrix of SeData is given as a binary matrix instead of using actual distances, we cannot get effective neighbors for kNN. Thus, kNN is not applied to SeData.

4.2 Experiment results

Kriging performance Table 1 shows the kriging performance of IGNNK and other baseline models on four datasets. As can be seen, the proposed method consistently outperforms other baseline models, providing the lowest RMSE and MAE on all datasets.

Table 1: Kriging performance comparison of different models on four datasets.

Model	METR-LA		NREL		USHCN		SeData	
	RMSE	MAE	RMSE	MAE	RMSE	MAE	RMSE	MAE
IGNNK	9.048	5.941	3.261	1.597	3.205	2.063	6.863	4.241
kNN	11.071	6.927	4.192	2.850	3.400	2.086	-	-
KPMF	12.851	7.890	8.771	7.408	6.663	4.847	13.060	8.339
GLTL	9.668	6.559	4.840	3.372	5.047	3.396	6.989	4.285
sRMGCNN	14.581	9.047	8.361	6.445	5.844	4.621	9.381	5.718
OKriging	-	-	3.470	2.381	3.231	1.999	-	-

As can be seen, IGNNK achieves good performance on the two spatial datasets—NREL and USHCN—where OKriging fits the tasks very well. There are two cases worth mentioning in Table 1. First, kNN and OKriging also gives comparable results to IGNNK on USHCN data, the MAE of OKriging is even lower than the one of IGNNK. This is due to the fact that sensors have a high density and precipitation often shows smooth spatial variation (see Figure 6 in Appendix D). In this case, local spatial consistency might be powerful enough for kriging, and thus we do not see much improvement from IGNNK. For SeData, GLTL also shows good performance. A potential reason is the data limitation: the adjacency structure of SeData is given as a binary matrix of sensor connectivity (i.e., 1 if two sensors are neighbors next to each other on a highway segment, and 0 otherwise;). In this case, W only encodes the typology, instead of the full pairwise distance information as in other datasets. In fact, relative distance serves a critical role in the kriging task on a highway network due to the complex causal structures and dynamics of traffic flow [14]. As a results, we do expect IGNNK less powerful due to the lack of “distance” effect. We provide some examples of spatial and temporal visualizations of IGNNK and other baseline models in Appendix D.

Transfer learning performance We next demonstrate the transferability of IGNNK. Our experiments are based on three datasets—METR-LA, SeData, and PeMS-Bay—collected from three different highway networks using the same type of sensors (i.e., loop detector).

PeMS-Bay dataset is very similar to METR-LA: both datasets register traffic speed with a 5-min frequency, and both of them provide travel distance for each of sensors. The two datasets are used side by side in [14]. SeData has the same format; however, as mentioned, the dataset provides a simple binary adjacency matrix showing connectivity. To show the effect of adjacency matrix, we train two sets of models separately following the approach as the kriging experiments: one with a Gaussian kernel adjacency matrix based on pairwise travel distance (same as METR-LA), and the other on the binary connectivity matrix (same as SeData).

The top part of Table 2 shows the results obtained using Gaussian kernel adjacency (*Gaussian*) and binary adjacency (*Binary*), respectively. Not surprisingly, IGNNK-Gaussian offers the best accuracy, clearly outperforming all other models. In general, *Gaussian* offers better performance than *Binary* for all the baseline models except sRMGCNN. Similar to the kriging experiment on SeData, we find *Binary* IGNNK and *Binary* GLTL demonstrate comparable performance.

Table 2: Kriging performance of different models on PeMS-Bay. The last two rows shows the transferability of the two IGNNK models trained on METR-LA and SeData.

Model	Gaussian			Binary		
	RMSE	MAE	MAPE	RMSE	MAE	MAPE
IGNNK	6.093	3.663	8.16%	9.245	5.394	13.26%
kNN	7.431	4.245	9.13%	-	-	-
KPMF	7.332	4.293	9.21%	10.065	5.985	16.03%
GLTL	8.846	4.486	10.25%	8.504	4.962	12.24%
sRMGCNN	13.460	10.318	21.41%	13.191	8.718	19.59%
IGNNK Transfer	METR-LA			SeData		
	6.713	4.173	9.19%	11.484	6.456	15.10%

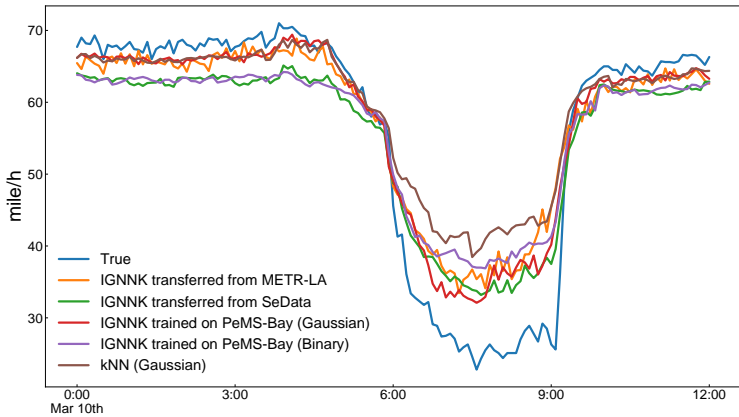


Figure 3: Kriging performance on unknown nodes in PeMS-Bay dataset. We provide the full baseline comparison in Appendix D.

We then apply the two IGNNK models—trained on METR-LA and SeData, respectively—directly on the test data of PeMS-Bay and obtain the kriging errors (the last two rows in Table 2). As can be seen, IGNNK (METR-LA) provides comparable performance to, if not better than, the second-best model—*Gaussian* GLTL; however, IGNNK (SeData) does not offer an encouraging results in this case. Our experiment shows that IGNNK can effectively learn the effect of pairwise distance from METR-LA and then generalize the results to PeMS-Bay. Figure 3 shows an example of kriging results of these models. While no models can reproduce the sudden drop during 6:00 am–9:00 am, we can see that *Gaussian* provides much better recovery during non-peak hours than *Binary*. The analysis on transferability further confirms the critical role of distance in kriging tasks.

5 Conclusion

In this paper, we introduce IGNNK as a novel framework for spatiotemporal kriging. Instead of learning transductive latent features, the training scheme provides IGNNK with additional generalization and inductive power. Thus, we can apply a trained model directly to perform kriging for any new locations of interest without retraining. Our numerical experiments show that IGNNK consistently outperforms other baseline models on five real-world spatiotemporal datasets. Besides, IGNNK demonstrates remarkable transferability in our traffic data kriging task as an example. Our results also suggest that “distance” information in graph plays a critical role in spatiotemporal kriging, which is different from applications in recommender systems where a graphs essentially encode topological information. The flexibility of this model allows us to model time-varying systems, such as moving sensors (e.g., probe vehicles) or crowdsourcing systems, which will create a dynamic network structure.

There are several directions for future work. First, we can adapt IGNNK to accommodate multivariate datasets as a spatiotemporal tensor (e.g., [2]). Second, better temporal models, such as RNNs and TCNs, can be incorporated to characterize complex temporal dependencies. This will allow us to perform kriging for a much longer time window with better temporal dynamics. Third, one can further combine time series forecasting with kriging in an integrated framework, providing forecasting results for both existing and virtual sensors for better decision making.

Acknowledgments and Disclosure of Funding

This research is supported by the Natural Sciences and Engineering Research Council (NSERC) of Canada, Fonds de recherche du Québec - Nature et technologies (FRQNT), and the Canada Foundation for Innovation (CFI). Y. Wu would like to thank the Institute for Data Valorisation (IVADO) for providing scholarship to support this study. The authors declare no competing financial interests with respect to this work.

References

- [1] Noel Cressie and Christopher K Wikle. *Statistics for Spatio-temporal Data*. John Wiley & Sons, 2015.
- [2] Mohammad Taha Bahadori, Qi Rose Yu, and Yan Liu. Fast multivariate spatio-temporal analysis via low rank tensor learning. In *Advances in Neural Information Processing Systems*, pages 3491–3499, 2014.
- [3] Syama Sundar Rangapuram, Matthias W Seeger, Jan Gasthaus, Lorenzo Stella, Yuyang Wang, and Tim Januschowski. Deep state space models for time series forecasting. In *Advances in Neural Information Processing Systems*, pages 7785–7794, 2018.
- [4] David Salinas, Michael Bohlke-Schneider, Laurent Callot, Roberto Medico, and Jan Gasthaus. High-dimensional multivariate forecasting with low-rank gaussian copula processes. In *Advances in Neural Information Processing Systems*, pages 6824–6834, 2019.
- [5] Rajat Sen, Hsiang-Fu Yu, and Inderjit S Dhillon. Think globally, act locally: A deep neural network approach to high-dimensional time series forecasting. In *Advances in Neural Information Processing Systems*, pages 4838–4847, 2019.
- [6] Christopher KI Williams and Carl Edward Rasmussen. *Gaussian Processes for Machine Learning*. The MIT Press, 2006.
- [7] Tinghui Zhou, Hanhuai Shan, Arindam Banerjee, and Guillermo Sapiro. Kernelized probabilistic matrix factorization: Exploiting graphs and side information. In *Proceedings of the SIAM International Conference on Data mining*, pages 403–414, 2012.
- [8] Dingxiong Deng, Cyrus Shahabi, Ugur Demiryurek, Linhong Zhu, Rose Yu, and Yan Liu. Latent space model for road networks to predict time-varying traffic. In *Proceedings of the 22nd ACM SIGKDD International Conference on Knowledge Discovery and Data Mining*, pages 1525–1534, 2016.
- [9] Koh Takeuchi, Hisashi Kashima, and Naonori Ueda. Autoregressive tensor factorization for spatio-temporal predictions. In *IEEE International Conference on Data Mining (ICDM)*, pages 1105–1110, 2017.
- [10] Keyulu Xu, Weihua Hu, Jure Leskovec, and Stefanie Jegelka. How powerful are graph neural networks? *arXiv preprint arXiv:1810.00826*, 2018.
- [11] Will Hamilton, Zhitao Ying, and Jure Leskovec. Inductive representation learning on large graphs. In *Advances in Neural Information Processing Systems*, pages 1024–1034, 2017.
- [12] Petar Veličković, Guillem Cucurull, Arantxa Casanova, Adriana Romero, Pietro Lio, and Yoshua Bengio. Graph attention networks. *arXiv preprint arXiv:1710.10903*, 2017.
- [13] Hanqing Zeng, Hongkuan Zhou, Ajitesh Srivastava, Rajgopal Kannan, and Viktor Prasanna. Graphsaint: Graph sampling based inductive learning method. In *International Conference on Learning Representations*, 2020.
- [14] Yaguang Li, Rose Yu, Cyrus Shahabi, and Yan Liu. Diffusion convolutional recurrent neural network: Data-driven traffic forecasting. *arXiv preprint arXiv:1707.01926*, 2017.

- [15] Juan C Martínez Mori and Samitha Samaranyake. Bounded asymmetry in road networks. *Scientific Reports*, 9:11951, 2019.
- [16] Nikhil Rao, Hsiang-Fu Yu, Pradeep K Ravikumar, and Inderjit S Dhillon. Collaborative filtering with graph information: Consistency and scalable methods. In *Advances in Neural Information Processing Systems*, pages 2107–2115, 2015.
- [17] Gabriel Appleby, Linfeng Liu, and Li-Ping Liu. Kriging convolutional networks.
- [18] Joan Bruna, Wojciech Zaremba, Arthur Szlam, and Yann Lecun. Spectral networks and locally connected networks on graphs. In *International Conference on Learning Representations*, 2014.
- [19] Michaël Defferrard, Xavier Bresson, and Pierre Vandergheynst. Convolutional neural networks on graphs with fast localized spectral filtering. In *Advances in Neural Information Processing Systems*, pages 3844–3852, 2016.
- [20] Thomas N Kipf and Max Welling. Semi-supervised classification with graph convolutional networks. *arXiv preprint arXiv:1609.02907*, 2016.
- [21] Youngjoo Seo, Michaël Defferrard, Pierre Vandergheynst, and Xavier Bresson. Structured sequence modeling with graph convolutional recurrent networks. In *International Conference on Neural Information Processing*, pages 362–373. Springer, 2018.
- [22] Bing Yu, Haoteng Yin, and Zhanxing Zhu. Spatio-temporal graph convolutional networks: A deep learning framework for traffic forecasting. pages 3634–3640, 2018.
- [23] Jiani Zhang, Xingjian Shi, Junyuan Xie, Hao Ma, Irwin King, and Dit-Yan Yeung. GaAN: Gated attention networks for learning on large and spatiotemporal graphs. *arXiv preprint arXiv:1803.07294*, 2018.
- [24] Zonghan Wu, Shirui Pan, Guodong Long, Jing Jiang, and Chengqi Zhang. Graph wavenet for deep spatial-temporal graph modeling. In *International Joint Conference on Artificial Intelligence*, pages 1907–1913, 2019.
- [25] Jiani Zhang, Xingjian Shi, Shenglin Zhao, and Irwin King. STAR-GCN: Stacked and reconstructed graph convolutional networks for recommender systems. *arXiv preprint arXiv:1905.13129*, 2019.
- [26] Muhan Zhang and Yixin Chen. Inductive matrix completion based on graph neural networks. *arXiv preprint arXiv:1904.12058*, 2019.
- [27] Federico Monti, Michael Bronstein, and Xavier Bresson. Geometric matrix completion with recurrent multi-graph neural networks. In *Advances in Neural Information Processing Systems*, pages 3697–3707, 2017.
- [28] Manajit Sengupta, Yu Xie, Anthony Lopez, Aron Habte, Galen Maclaurin, and James Shelby. The national solar radiation data base (NSRDB). *Renewable and Sustainable Energy Reviews*, 89:51–60, 2018.
- [29] Matthew J Menne, Claude N Williams Jr, and Russell S Vose. The US historical climatology network monthly temperature data, version 2. *Bulletin of the American Meteorological Society*, 90(7):993–1008, 2009.
- [30] Zhiyong Cui, Ruimin Ke, and Yinhai Wang. Deep bidirectional and unidirectional LSTM recurrent neural network for network-wide traffic speed prediction. *arXiv preprint arXiv:1801.02143*, 2018.
- [31] Daniel G Krige. A statistical approach to some basic mine valuation problems on the witwatersrand. *Journal of the Southern African Institute of Mining and Metallurgy*, 52(6):119–139, 1951.
- [32] Kathleen M Carley, Dave Columbus, and Ariel Azoulay. Automap user’s guide 2012. Technical report, CARNEGIE-MELLON UNIV PITTSBURGH PA INST OF SOFTWARE RESEARCH INTERNAT, 2012.
- [33] Sungyong Seo and Yan Liu. Differentiable physics-informed graph networks. *arXiv preprint arXiv:1902.02950*, 2019.

A Data description

We use five real-world spatiotemporal datasets to assess our model (see Table 3 for a summary). They are:

METR-LA¹ contains traffic speed information collected by highway loop detectors in Los Angeles [14]. We follow the work of Li et al. [14] to select 4 months of data from 207 sensors with 5-min frequency from Mar 1st 2012 to Jun 30th 2012. For “0” entries in X (missing values), the corresponding entries in the mask matrices also set to 0. We build the adjacency matrix following [14]:

$$W_{ij} = \exp\left(-\left(\frac{\text{dist}(v_i, v_j)}{\sigma}\right)^2\right), \quad (5)$$

where W_{ij} is the adjacency matrix weights between sensors v_i and v_j , $\text{dist}(v_i, v_j)$ represents the road network distance and $\sigma = 6696$ m is the standard deviation of sensor distances. We further set $W_{ij} = 0$ if $W_{ij} < 0.1$. The final adjacency matrix is obtained directly from Github repository of [14].

NREL² provides several energy datasets, and here we choose the Alabama Solar Power Data for Integration Studies [28]. The solar power data contain 5-minute solar power collected by 137 photovoltaic power plants in 2006. Similarly, we follow [2] and use the following formulation to construct the adjacency matrix given the geometric distances between power plants:

$$W_{ij} = \exp\left(-\frac{\text{dist}(v_i, v_j)}{\sigma}\right), \quad (6)$$

where $\text{dist}(v_i, v_j)$ is calculated using the Haversine formula based on longitude and latitude. We set $\sigma = 7.5$ km. The maximum capacities of each power plant are provided in this dataset. In each node, each time series is normalized to $[0,1]$ by dividing the values by the corresponding capacity. In this dataset, half of the observations are zeros due to sunrise and sunset. The zero observations will undermine the training of both IGNNK and other baseline models. To alleviate this effect, we only keep the data from 7 am–7 pm each day. Note that we regard “0” entries in NREL as true observations. Therefore, we do not impose additional masks for missing values when processing the data.

USHCN³ consists of 1218 time series of monthly precipitation from 1899 to 2019, which is collected by the U.S. Historical Climatology Network (USHCN) [29]. We apply the same rule as in NREL to construct dynamic adjacency matrix with $\sigma = 50$ km. We further set $W_{ij} = 0$ if $W_{ij} < 0.012$. As the time span of this dataset is much longer than others and the variance-to-mean ratio exceeds 500, the dataset can help examine how different models perform on time series with substantial oscillations.

SeData⁴ is also a traffic speed dataset. It registers 5-min traffic speed data from 323 loop detectors in Seattle highway of a year [30]. It should be noted that SeData does not provide exact coordinates and topology information of sensors. Instead, it provides a binary adjacency matrix based on neighborhood. We build the adjacency matrix using classical undirected graph definition:

$$W_{ij} = \begin{cases} 1, & \text{if } i \text{ and } j \text{ are neighbors,} \\ 0, & \text{otherwise.} \end{cases} \quad (7)$$

PeMS⁵ refers to Performance Measurement System (PeMS) for California highway. It is collected by California Transportation Agency (CalTrans). Same as the work of Li et al. [14], we select 325 sensors in the Bay Area (PeMS-Bay) between Jan 1st 2017 and May 13th 2017. The temporal frequency of PeMS-Bay is also 5-min. We use **PeMS-Bay** to demonstrate the transferability of IGNNK. The adjacency matrix construction will adapt the transfer learning task accordingly. The adjacency matrix construction for training IGNNK and transferring model trained on METR-LA is

¹<https://github.com/liyaguang/DCRNN>

²<https://www.nrel.gov/grid/solar-power-data.html>

³<https://www.ncdc.noaa.gov/ushcn/introduction>

⁴<https://github.com/zhiyongc/Seattle-Loop-Data>

⁵<https://github.com/liyaguang/DCRNN>

also Gaussian kernel given in Eq. (5). The final adjacency matrix is obtained from Github of [14]. For transferring IGNNK model trained on Sedata, we use the binary adjacency matrix given by Eq. (7). We summarize these dataset in Table 3.

Table 3: Real-world spatiotemporal datasets description

	Sensors	Time length (frequency)	Adjacency matrix	Usage	Missing
METR-LA	207	34272 (5-min)	Threshold Gaussian kernel	IGNNK training	8.11%
NREL	137	105120 (5-min)	Geo-distance Gaussian kernel	IGNNK training	-
USHCN	1218	1440 (1-month)	Geo-distance Gaussian kernel	IGNNK training	3.07%
SeData	323	105120 (5-min)	0-1 undirected graph	IGNNK training	-
PeMS-Bay	325	52116 (5-min)	Gaussian kernel	IGNNK training	0.003%
PeMS-Bay	325	52116 (5-min)	0-1 graph (SeData)	Transfer learning	0.003%
PeMS-Bay	325	52116 (5-min)	Gaussian kernel (METR-LA)	Transfer learning	0.003%

B Implementation details of IGNNK

Why use diffusion convolution: There exists a large number of works on GCN structures. We have compared diffusion convolution [14] with both GCN [20] and Chebynet [19]. We found that diffusion convolution outperforms the other 2 baselines. In addition, diffusion convolution is a structure specifically designed for spatiotemporal data and it can be applied on directed networks.

The parameters of GNNs: We use 3-layers DGCNs for experiments on different datasets. The parameters for training the GNNs are given in Table 4. The number of iteration I_{\max} is determined by the temporal length of each dataset: $I_{\max} \approx 750 \times \frac{0.7 \times T}{h \times S}$.

Table 4: IGNNK Parameters for each dataset

Parameters	METR-LA	NREL	USHCN	SeData	PeMS-Bay 0-1 / Gaussian
window length h	24	16	6	24	24
number of evaluation windows (test)	428	1971	72	1314	2171
number of kriging nodes (n_t^u)	50	30	300	80	80
sampled observed nodes size n_o	100	100	900	240	240
sampled masked nodes size n_m	50	30	300	80	80
hidden feature dimension z	100	100	100	350	100
activation function σ	<i>relu</i>	<i>relu</i>	<i>relu</i>	<i>relu</i>	<i>relu</i>
batch size (S)	4	8	8	4	4
number of iterations (I_{\max})	186750	287250	30750	574500	285000
order of diffusion convolution	2	2	2	2	2

We use Adam optimizer with learning rate 0.0001 to optimize the GNNs. Figure 4 shows the test RMSE curves METR-LA. We can see that test RMSE of DGCN is stable after 200 epochs of training without overfitting. We also plot the learning curves using 3 layers of GCN and Chebynet. For GCN, we use *selu* activation because it outperforms *relu* in our experiments. For Chebynet, the convolution order is set to 3.

Evaluation and real-time kriging: For model evaluation, we provide the information Y_t^s during time period $[t, t + h)$ of the new graph and mask unsampled nodes. We use the reconstruction errors on unsampled nodes Y_t^u for evaluation. We perform rolling recovery, e.g., $[t + h, t + 2h)$ with Y_{t+h}^s , and $[t + 2h, t + 3h)$ with Y_{t+2h}^s , using the same model on test data.

Evaluation on transfer learning performance: The PeMS-Bay data between Jan 1st 2017 and May 13th 2017 are used to evaluate the model. We apply the two trained models—IGNNK (METR-LA) and IGNNK (SeData) on the PeMS-Bay dataset with 80 evaluation sensors. Note that we also define and reconstruct the corresponding binary adjacency matrix W_{ij} when applying IGNNK (SeData).

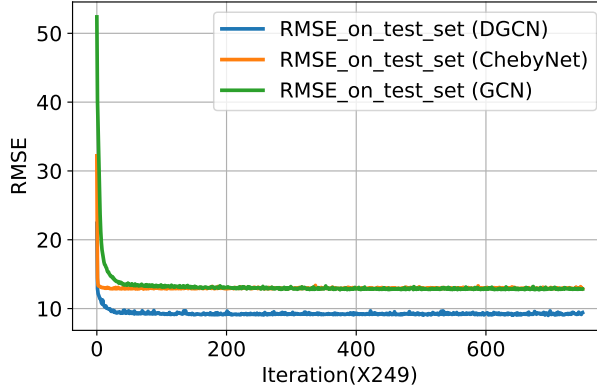


Figure 4: The learning RMSE curve on METR-LA test set.

Computing infrastructure description: We use Alienware R8 with CPU 8 core 3832.495 mHz, GPU GeForce RTX 2080 Ti 8GB, and 12GB memory for *Python*-based experiments. It tanks about 15min-30min to train a IGNNK, but depending on the datasets.

C Benchmark settings

C.1 Baseline models

kNN For METR-LA/PeMS-Bay, the distance is defined by the road distance in the transportation network. In NREL/USHCN, distance is defined by the Haversine distance. For each dataset, we select the best k by comparing the kriging RMSE errors. Based on that, we use inverse distance weight instead of simply averaging the K neighbors during prediction. Prediction $\hat{x} = \sum_{i=1}^K \frac{1}{d_i} x_i$, where d_i is the distance to between the unknown node and the corresponding observed neighbor. We choose the optimal K according to their lowest RMSE. The selection of k for different datasets follows: *METR-LA*: 7; *NREL*: 10; *USHCH*: 7 and *PeMS-Bay (Gaussian)*: 4.

OKriging Ordinary kriging is a geostatistical method that interpolates values by a Gaussian process governed by prior spatial covariance. We implement the ordinary kriging by *Automap* [31, 32]. *Automap* automates the process of kriging by adaptively fitting variograms and testing a number of different models. In our experimental setting, we test spherical, exponential, Gaussian, matern, and stein variograms and then picks the best one with the smallest residual sum of squares. Note that we apply the method separately for each snapshot window $[t, t + h)$ in the test data. In other words, at each time point t , we provide the corresponding column vector in Y_t^s to the algorithm to get the interpolated column vector as kriging result. This task can be embarrassingly parallel for all time points.

KPMF Kernelized Probabilistic Matrix Factorization [7] exploits graph kernel as side information to perform matrix completion. It can infer the rows/columns with no entries. It is originally designed for recommender systems, but it can be extended to spatiotemporal tasks. Given the input matrix with N sensors and T time points, we use the same adjacency matrices in Appendix A. to build the Laplacian graph kernels. We implement this model using the *MATLAB* code⁶ provided by the authors. We focus on its spatially kriging performance and impose identity matrix as temporal kernel. In the implementation, we use stochastic gradient descent for optimization, and set the learning rate and maximum number of iterations to 1×10^{-6} and 100, respectively. We perform grid search to tune three critical parameters using validation RMSE: *Variance* σ^2 : $\{0.001, 0.01, 0.1, 1, 10\}$, *Size of latent dimensions* D : $\{10, 20, 40, 80\}$ and *Graph weight* γ : $\{0.001, 0.01, 0.1, 1, 10\}$. The tuned parameters for KPMF are listed in Table 5.

GLTL Greedy Low-rank Tensor Learning [2] is a model for both cokriging and forecasting tasks for multiple variables. The number of variables is 1 for our datasets. We implement this using the

⁶<https://people.eecs.berkeley.edu/~tinghuiz/>

Table 5: KPMF Parameters for each dataset

Parameter	METR-LA	NREL	USHCN	Sedata	PeMS-Bay
σ^2	0.1	0.1	1	1	0.1
D	20	20	20	20	40
γ	0.01	1	0.01	0.1	0.1

MATLAB source code⁷ provided by the authors. We choose the *Orthogonal* algorithm as it shows superior performance in [2]. We set the maximum number of iterations to 100 and the convergence stopping criteria to 1×10^{-10} . For other datasets, we use the same adjacency matrices as IGNNK are used. For directed networks (i.e., METR-LA, SeData and PeMS-Bay), we set $W = (W + W^T) / 2$ to get the undirected version. The Laplacian matrix is computed by $L = D - W$ where D is a diagonal matrix with $D_{ii} = \sum_j W_{ij}$. Following the implementation in [2], we also rescale the Laplacian matrix by $L = \frac{L}{\max_{ij} L_{ij}}$. The other critical parameter is μ for the weight of Laplacian regularizer. We perform grid search by validation on the first 70% time points of the “unsampled” sensors. We choose μ from $\{0.05, 0.5, 5, 50, 500\}$. We reach convergence before 100 iterations on all datasets. The tuned parameters for different datasets are listed in Table 6.

Table 6: GLTL Parameters for each dataset

Parameter	METR-LA	NREL	USHCN	Sedata	PeMS-Bay
μ	0.5	50	5	5	5

sRMGCNN Separable Recurrent Multi-Graph CNN, it is a transductive matrix completion framework using GCNs to learn graph structures. We implement this using the source code in GitHub⁸. We need to define the possible largest entry value during training, which can be considered the highest rating in recommendation system. The highest values chosen for five datasets are: *METR-LA*: 80; *NREL*: 50; *USHCN*: 100; *SeData*: 80; *PeMS-Bay*: 80.

C.2 Implementation of matrix completion models

There are two approaches to apply the matrix completion models. The first approach is to train the models on the whole matrix of the datasets presented in Table 3. The second approach is to train and validate the model using first 70% time points to get optimal parameters, and then train another model on the 30% test with the optimal parameters. Both approaches can provide the whole reconstruction/interpolation at once. For all the transductive matrix completion models, we find that the first approach that uses the information of all the time points (i.e., whole matrix) provides better results than the second one. The reason is that the first approach can leverage historical information, while the second approach cannot. We implement all algorithms using a workstation with a Xeon E5-2698v4 CPU and a Tesla V100 GPU.

C.3 Evaluation metrics

We use the following metrics to compare model performance.

Root Mean Square Error (RMSE):

$$\text{RMSE}(x, \hat{x}) = \sqrt{\frac{1}{|N|} \sum_{i \in N} (x_i - \hat{x})^2}.$$

Mean Absolute Error (MAE):

$$\text{MAE}(x, \hat{x}) = \frac{1}{|N|} \sum_{i \in N} |x_i - \hat{x}|.$$

⁷<http://roseyu.com/code.html>

⁸<https://github.com/fmonti/mgcn>

Mean Absolute Percentage Error (MAPE):

$$\text{MAPE}(x, \hat{x}) = \sum_{i \in N} \left| \frac{x_i - \hat{x}}{x_i} \right|.$$

D Visualization of result

We provide spatial and temporal visualizations to show the performing of IGNNK. For spatial visualization, we select crowded/uncrowded periods to examine the performance of our model on capturing the sharp peaks and fitness the trends.

Spatial visualization

Since SeData has no geographical information, we cannot plot its sensor locations. In Figures 5, 6 and 7, we depict the spatial visualizations for METR-LA, USHCN and NREL datasets.

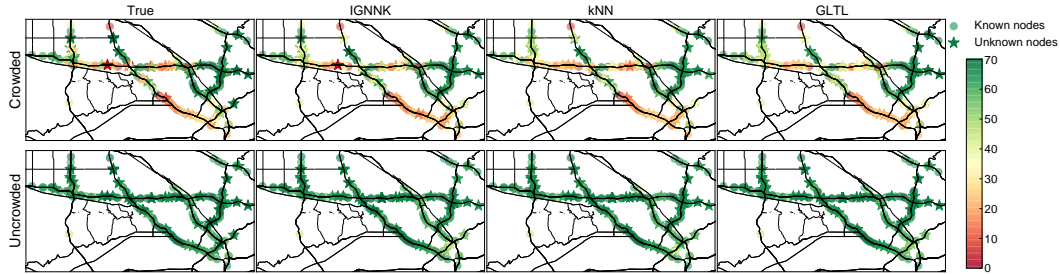


Figure 5: Spatial presentation of kriging performance in crowded and uncrowded time upon METR-LA dataset. Compared models are ground truth, IGNNK, kNN, GLTL (from left to right in each row).

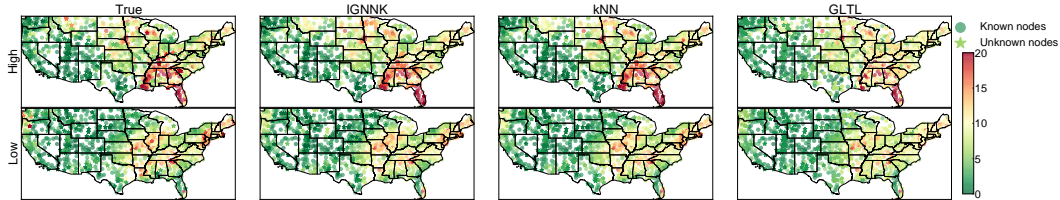


Figure 6: Spatial visualization of kriging performance in high and low precipitation time for USHCN dataset.

For all figures, we select the crowded/high precipitation/noon time to illustrate the performance of IGNNK in capturing peak as well as the uncrowded/low precipitation/evening time to discover the fitness in trends. It can be found that IGNNK consistently outperforms other baseline models. The evaluation metrics can be found in Table 1.

Temporal visualization

Figure 8 gives the temporal visualization of kriging results. For each dataset, we select a certain time window to demonstrate the performance of different models. As can be seen, IGNNK provides better fit to the true data than other baseline models.

Transfer learning temporal visualization

Figure 9 shows results for transfer learning tasks. We select one of the unknown sensors in PeMS-Bay as an example. Figure 9(a) shows a period when IGNNK outperforms kNN. Figure 9(b) gives another period when kNN performs better than IGNNK. In both examples, we show the results from the transferred models. As can be seen, the transferred models from METR-LA and SeData provide comparable performance, if not better than, GLTL as the best transductive model. This results verifies that our model can indeed learn the inductive message passing mechanism. Detailed quantitative results can be found in Table 2.

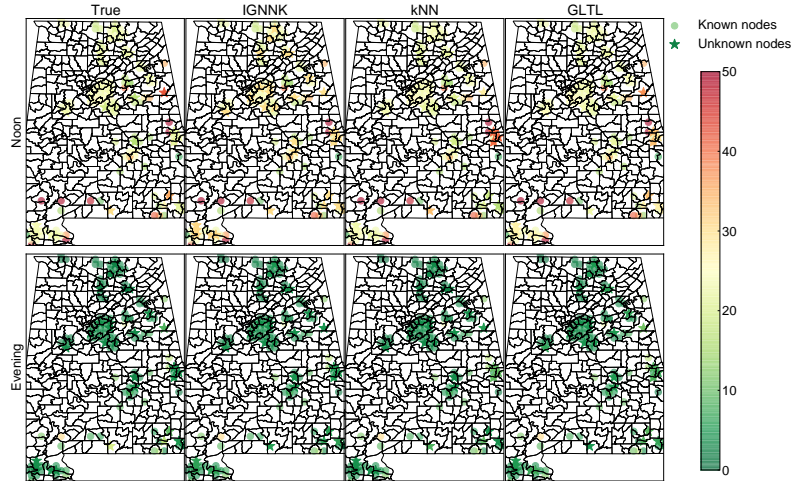


Figure 7: Spatial visualization of kriging performance in noon and evening time for NREL solar system in Alabama state.

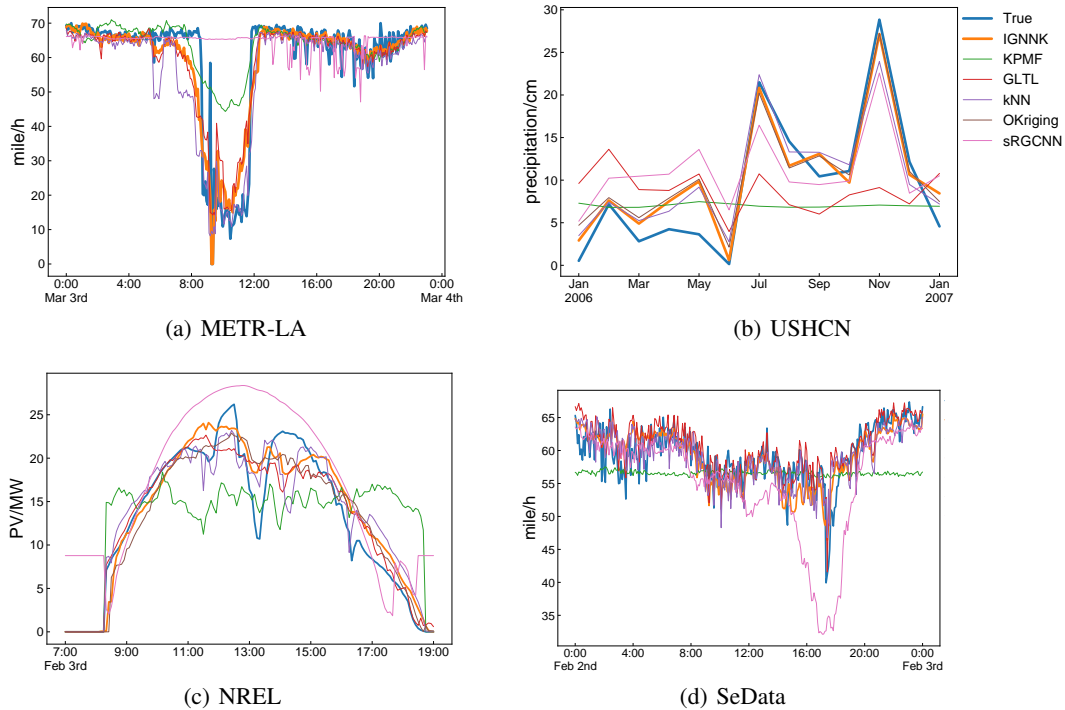


Figure 8: Temporal visualization of kriging results.

Neural Network Weights Visualization

To better illustrate the generalization ability for transfer learning and the power of diffusion process, we visualize the network weights Θ in Eq (1) of three DGCN layers, as can be found in Figure 10. We set models with the same adjacency matrix together and average the parameters to make them equally sized. It can be found that even though the parameters in the first layer greatly differ from the other, they ultimately tend to be similarly distributed. This gives us an intuitive understanding of why transfer learning works because the message passing mechanism is learned by a deep GNN. Furthermore, it can be found in Figure 10(c) that models with binary adjacency tend to be sharper than

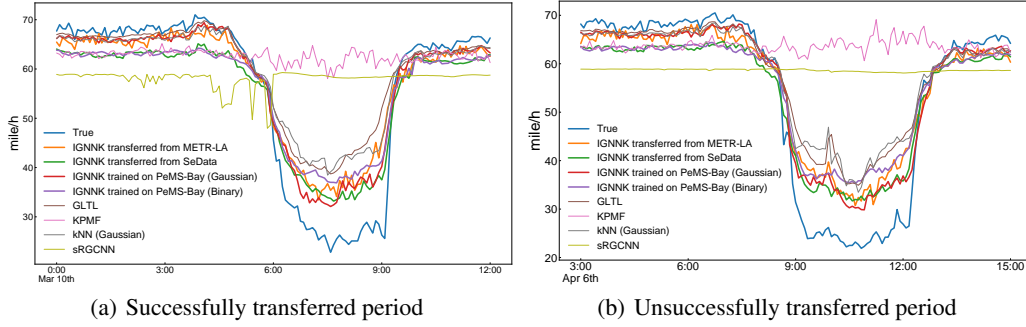


Figure 9: Kriging performance on unknown nodes in PeMS-Bay dataset with all the baseline models.

Gaussian kernel based ones. This might explain why they are less accurate than the Gaussian kernel based models, as they focus more on the local smoothness and capture less long-range information.

E Explanation with Partial Differential Equation

Many real-world dynamic systems can be represented as a relation between temporal and spatial derivatives:

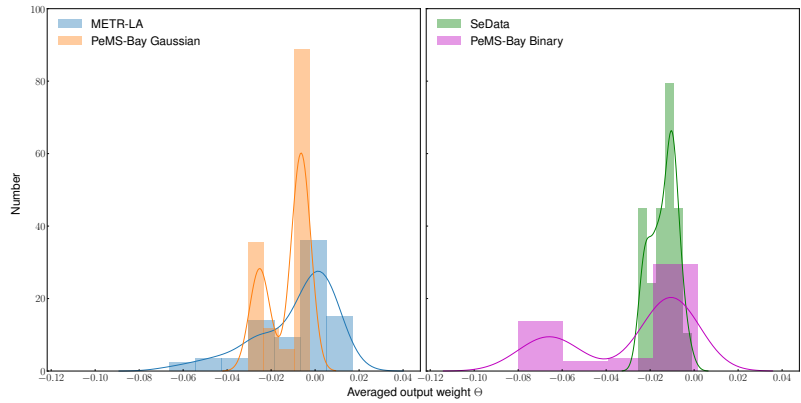
$$\sum_{i=1}^M \frac{\partial^i u}{\partial t^i} = \sum_{i=1}^N a_i(u, x) \frac{\partial^i u}{\partial x^i}, \quad (8)$$

where u is a physical quantity (e.g. traffic speed and precipitation). x is the spatial direction, and t is the time point. M and N are the highest order of temporal derivatives and spatial derivatives, respectively. It is suggested that any type of Partial Differential Equation (PDE) written in Equation 8 can be represented by a graph neural networks [33].

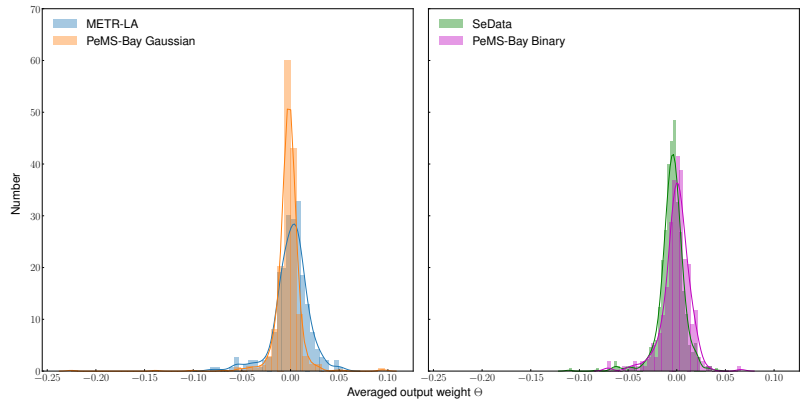
To perform spatiotemporal kriging, we are particular interested in how the target physical quantity u varies over spatial direction. As stated before, we have modeled the interaction of u in temporal direction as fully connected neural networks. The continuous version of the simplified IGNNK model (1-layer) can be represented as the following PDE

$$u(x, t) = L \frac{\partial a(u(x, t))}{\partial x}, \quad (9)$$

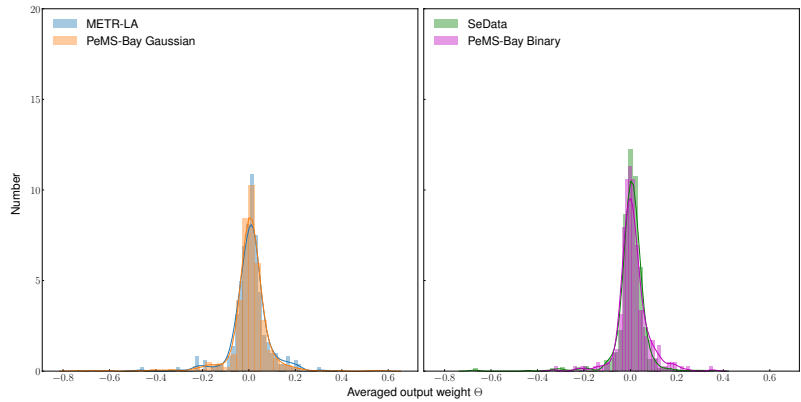
where L is the Laplace operator determined by the used GNN structure. $a(u(x, t))$ is a function represented by a fully connected neural networks. The goal is to get the parameters of function $a()$, then the physical quantity u at unknown xs can be estimated.



(a) Diffusion learning parameter Θ in the first layer DGCN



(b) Diffusion learning parameter Θ in the second layer DGCN



(c) Diffusion learning parameter Θ in the third layer DGCN

Figure 10: Visualization of learning parameters in three DGCN layers.